Solar Phys (2011) 269: 367–388
DOI 10.1007/s11207-010-9699-9

Coronal Field Opens at Lower Height During the Solar Cycles 22 and 23 Minimum Periods: IMF Comparison Suggests the Source Surface Should Be Lowered

C.O. Lee · J.G. Luhmann · J.T. Hoeksema · X. Sun · C.N. Arge · I. de Pater

Received: 5 June 2010 / Accepted: 7 December 2010 / Published online: 7 January 2011

Abstract The solar cycle 23 minimum period has been characterized by a weaker solar and interplanetary magnetic field. This provides an ideal time to study how the strength of the photospheric field affects the interplanetary magnetic flux and, in particular, how much the observed interplanetary fields of different cycle minima can be understood simply from differences in the areas of the coronal holes, as opposed to differences in the surface fields within them. In this study, we invoke smaller source surface radii in the potential-field source-surface (PFSS) model to construct a consistent picture of the observed coronal holes and the near-Earth interplanetary field strength as well as polarity measurements for the cycles 23 and 22 minimum periods. Although the source surface value of 2.5 $R_\odot$ is typically used in PFSS applications, earlier studies have shown that using smaller source surface heights generates results that better match observations during low solar activity periods. We use photospheric field synoptic maps from Mount Wilson Observatory (MWO) and find that the values of ≈ 1.9 $R_\odot$ and ≈ 1.8 $R_\odot$ for the cycles 22 and 23 minimum periods, respectively, produce the best results. The larger coronal holes obtained for the smaller source surface radius of cycle 23 somewhat offsets the interplanetary consequences of the lower magnetic field at their photospheric footpoints. For comparison, we also use observations from the Michelson Doppler Imager (MDI) and find that the source surface radius of ≈ 1.5 $R_\odot$ produces better results for cycle 23, rather than ≈ 1.8 $R_\odot$ as suggested from MWO observations. Despite this difference, our results obtained from MWO and MDI observations show a qualitative consistency regarding the origins of the interplanetary field

C.O. Lee (✉) · J.G. Luhmann
Space Sciences Laboratory, University of California, Berkeley, CA, USA
e-mail: clee@ssl.berkeley.edu

C.O. Lee · I. de Pater
Department of Earth and Planetary Science, University of California, Berkeley, CA, USA

J.T. Hoeksema · X. Sun
W. W. Hansen Experimental Physics Laboratory, Stanford University, Stanford, CA, USA

C.N. Arge
Air Force Research Laboratory/Space Vehicles Directorate, Kirtland Air Force Base, NM, USA

and suggest that users of PFSS models may want to consider using these smaller values for their source surface heights as long as the solar activity is low.

Keywords Corona, models · Coronal holes · Magnetic field, interplanetary · Magnetic field, observations · Solar cycle, observations

1. Introduction

The solar cycle 23 deep solar minimum period is unlike the corresponding phases of the previous two solar cycles. Ground-based magnetograph observations from the Wilcox Solar Observatory (WSO) shown in Figure 1 reveal that the solar field is reduced over the entire surface of the Sun, while the polar field values are about half those observed during the previous minimum period (Hoeksema, 2010). These weaker solar fields resulted in changes in the bulk properties of the interplanetary medium. In-ecliptic, near-Earth observations during the declining-to-minimum phase of cycle 23 showed that the interplanetary magnetic field (IMF) strength (Figure 2) and solar wind density were about 30% lower, whereas the momentum flux was about 38% lower, but the solar wind speeds remain unchanged (Lee *et al.*, 2009b). The *Ulysses* (Balogh *et al.*, 1992; Bame *et al.*, 1992) off-ecliptic observations for the same solar cycle period revealed similar changes throughout the heliospheric medium, including a reduction of the radial magnetic field by about 64% , dynamic pressure by about 22%, and thermal pressure by about 25% (Smith and Balogh, 2008; McComas *et al.*, 2008).

The weaker solar field and IMF of the cycle 23 minimum period makes it an ideal time to understand how the solar field maps into interplanetary space to control the observed IMF. In the past, different methods have been used to compute the IMF strength from the photospheric field (see, *e.g.*, Levine *et al.* (1977), Zhao and Hoeksema (1995), Wang, Robbrecht, and Sheeley (2009) and references therein). In this study, we take a somewhat different approach to compare the computed IMF strength with observations by considering different source surface heights in the well-known potential-field source-surface (PFSS) model of the coronal magnetic field (Schatten, Wilcox, and Ness, 1969; Altschuler and Newkirk, 1969). Our goal is to build a coherent picture of the coronal holes and their footpoint magnetic field as well as the interplanetary field and polarity measurements for the two most recent solar minima. In particular, we investigate *i*) how the strength of the photospheric field modifies the magnetic flux coming from the Sun, and *ii*) how much of the recent weak IMF can be understood simply from changes in the coronal holes.

The PFSS model, which has been widely used for decades to study interplanetary field and photospheric sources of the solar wind, provides a snapshot of the open coronal field regions. Because the model is based on photospheric magnetic field synoptic maps that are assembled from full-disk magnetograms obtained over a solar rotation, it can capture many details of the global field geometry, especially when the Sun is in the quiet phases of its activity cycle (see, *e.g.*, Levine *et al.*, 1977). The outer boundary of the PFSS model is usually a spherical source surface of about 1.5 to 3.5 solar radii ($R_{\odot}$) located at a constant height above the inner boundary at the photosphere. At the source surface, the field is radial. It is assumed that between the photosphere and the source surface the coronal field is current-free. Even with the current-free and spherical source surface assumptions, the PFSS model can generate solutions that closely match those generated by the physics-based magnetohydrodynamic (MHD) models for cases when time-dependent phenomena are negligible during both the solar minimum and maximum periods (Riley *et al.*, 2006).

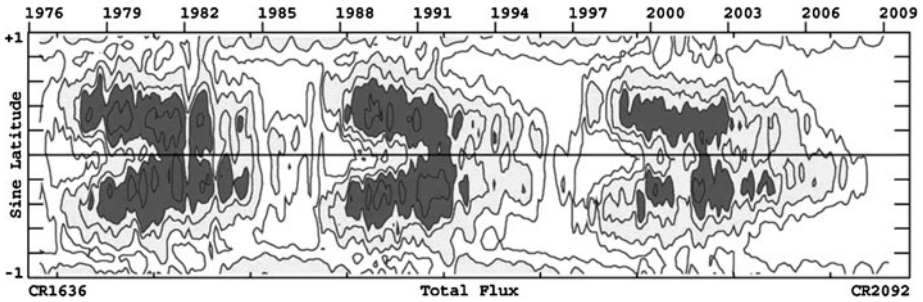

Figure 1 Observed total photospheric magnetic flux (longitudinally averaged) for solar cycles 21, 22, and 23. The contour levels are for magnetic field values of 50, 100, 200, 300, 500, and 1000 μT (100 μT = 1 G), where the two strongest contours are shaded in dark gray and the two weakest contours are shown in white. The density and color of the contours suggests a weaker overall solar surface field for the cycle 23 minimum period compared to the previous ones. Image credit: Stanford University Wilcox Solar Observatory.

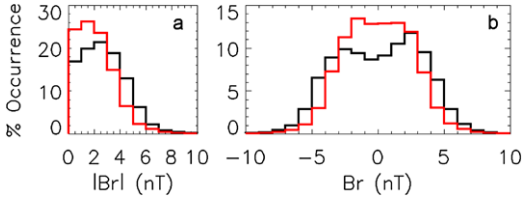

Figure 2 Histogram of occurrence for the (a) unsigned and (b) signed radial magnetic field observed near Earth during the cycle 22 (black) and cycle 23 (red) minimum periods.

Recently, Wang, Robbrecht, and Sheeley (2009) used the PFSS model with a fixed source surface height of 2.5 $R_\odot$ together with a current sheet correction and synoptic map evolution model to analyze how the weak IMF can result from a reduction in flux emergence rates together with adjusted flux redistribution parameters. They concluded that slightly faster meridional flows would be sufficient to produce the observed weaker IMF from the observed rate of flux emergence in active regions. On the other hand, Levine (1982), Levine *et al.* (1977), and Hoeksema, Wilcox, and Scherrer (1983) discuss the possible influence of different source surface heights on the mapping of the solar magnetic field into the interplanetary medium. Although the source surface value of 2.5 $R_\odot$ is typically used in PFSS applications, the value which has been tuned to match the IMF polarity pattern (see Hoeksema, Wilcox, and Scherrer, 1983), Schatten, Wilcox, and Ness (1969), Levine (1982), and Levine *et al.* (1977) found that using smaller source surface heights generated PFSS results that better matched observations of open magnetic fields during periods of low solar activity. A reduction in the source surface height for this minimum period would be consistent with the coronal MHD simulations of Steinolfson, Suess, and Wu (1982), which showed the expected relationship between photospheric field strength and streamer belt height (see Figure 11 in their study).

The main objective in our study is to explore the assumption of Schatten, Wilcox, and Ness (1969), Levine *et al.* (1977), and Levine (1982) that the source surface height should be treated as a free parameter in PFSS modeling. The theoretical implication is that the strength of the IMF should be influenced by the radial extent of the closed field regions in the corona as indicated in the MHD models. Our study is also complementary to the study by Wang, Robbrecht, and Sheeley (2009) in that it calls attention to another parameter to be considered in such studies. Last but not least, our study seeks to explain why this past cycle's solar minimum interplanetary field has assumed its particular magnitude.

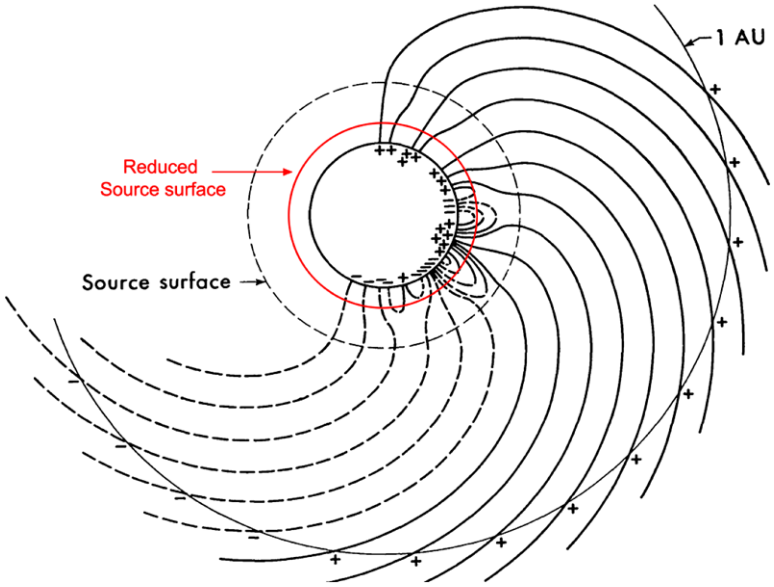

Figure 3 Cartoon illustrating that a smaller source surface will encompass more open field lines and enlarge the coronal hole areas from which the open field emanates. Note that the number of polarity reversals also increases. Figure adapted from Schatten, Wilcox, and Ness (1969).

2. Approach

Over the years, the PFSS model has been refined by Hoeksema (1984) and Wang and Sheeley (1992), and its strengths and weaknesses have been explored in studies such as those by Riley *et al.* (2006). We use the version of the PFSS model that has been documented in a previous report by Luhmann *et al.* (2002), which is currently available for running at the Community Coordinated Modeling Center (CCMC, http://ccmc.gsfc.nasa.gov). For this study, the model uses a uniform grid of 60 × 120 ($\theta \times \phi$) grid points, where the spacings in the θ and ϕ directions are both 3°. As Riley *et al.* (2006) demonstrated, the PFSS model is especially applicable during the solar minimum period. Since there is less activity and fewer currents at this time, the potential field is a better approximation of the open field coronal holes on the photosphere. We use the spherical harmonic coefficients derived from the Mount Wilson Observatory (MWO) synoptic photospheric field maps, which are processed in the manner described by Arge and Pizzo (2000), Ulrich *et al.* (2002), and Arge *et al.* (2004). Twenty orders of spherical harmonic coefficients are sufficient to capture the bulk of the important photospheric features and their coronal effects for our solar minimum study period.

In this study we utilize the source surface height as a means of controlling the amount of solar photospheric flux that maps into the interplanetary medium. As illustrated in Figure 3, by reducing the source surface height in the PFSS model, more of the flux extends into the interplanetary medium as more coronal field structures become open (*i.e.*, the source surface will intersect more previously closed field lines) and the photospheric areas from which the open structures emanate become larger. The implication is that what is observed in interplanetary space is a consequence of the photospheric field strength, the distribution of the magnetic flux, and the height where the last closed photospheric field lines, and thus the source surface height, occur.

A few assumptions are made in using the PFSS model to characterize the amount of open flux in the heliosphere for the cycles 22 and 23 minimum periods. It is implicitly assumed that all the open (interplanetary) magnetic flux comes from the coronal hole footpoints identified by the PFSS model. Note that we do not include a current sheet with its associated field, which is in contrast to other PFSS-based studies (*e.g.*, Wang, Robbrecht, and Sheeley, 2009) that use this Schatten current sheet correction (see Schatten, 1971). Without the inclusion of a current sheet, the spatial distribution of flux at the source surface does not match the uniform distribution of the field strength observed in the IMF. We also assume that there is no significant heliospheric flux contribution from interplanetary coronal mass ejections, which is reasonable given that our period of study is the solar cycle minimum. To relate the computed open flux at the Sun to the observed radial IMF at 1 astronomical unit (AU), we assume that the IMF magnitude is independent of heliographic latitude (see Balogh *et al.*, 1995) and thus varies in proportion to the amount of open flux (*e.g.*, Smith and Balogh, 2008).

We also note that corrections applied to the line-of-sight (LOS) polar field measurements in the MWO synoptic maps can affect the computed open flux values presented in this study. All of the maps used here have had a "correction" applied to the polar field data in the hemisphere directed away from Earth, as this is where the LOS measurements are typically highly unreliable or even missing from the maps. The main idea behind this (retrospective) correction method is to use polar field observations *i*) during periods when they are well observed (*i.e.*, when they are directed nearly at maximum toward the Earth) and *ii*) that span a time interval long before and after the period (*i.e.*, synoptic map) of interest. A second-order polynomial curve is fitted to these data, and the difference between the average of the polar field data in the hemisphere of the map directed away from the Earth and the polynomial fit is determined. This difference is then added as a uniform offset to the polar field being corrected so that its average value is the same as that determined from the fit (see Arge and Pizzo, 2000 for details). Modifying the polar field in this manner will change the amount and distribution of the PFSS-computed open and closed flux. The differences are usually modest in comparison to those that occur when the correction is not applied.

In general, by using the MWO solar observations to calculate the open flux, we acknowledge that the absolute levels of flux can vary from those calculated using solar field measurements taken at other observatories. The variations can be due partly to the spatial resolution of the observations, calibration techniques of the instrument, corrections applied to the data (*e.g.*, for spectral line saturation effects or the aforementioned LOS polar field measurements), and other factors. In a previous study, Arge *et al.* (2002) used the photospheric magnetic field measurements from the Mount Wilson, Wilcox, and National Solar Observatories (MWO, WSO, and NSO, respectively) to calculate the total photospheric flux and the open flux using the PFSS model (source surface $= 2.5\ R_{\odot}$). Detailed corrections and modifications were applied to each set of observations, including the interpolation of the synoptic maps to a common and uniform grid since the spatial resolution of the data from each observatory was different (in increasing order: WSO, MWO, and NSO). With these corrections and modifications applied to the observations, they were able to more directly intercompare the total photospheric and open solar fluxes based on the different solar observations. Despite the uncertainties and differences of each data set, they found that the integrated flux results from each observatory agreed very well during the solar minima periods (for our cycle 22 minimum study period, the agreement is within roughly 15% for the photosphere and roughly 20% for the source surface based on the data shown in Figures 1 and 3b, respectively, in Arge *et al.* (2002)). In this two-solar-cycle (minimum periods) study, there are several advantages to using the synoptic maps from MWO *versus* those from NSO

or WSO. One advantage is that the MWO instrumentation has been relatively stable and consistent since around 1992 (Arge *et al.*, 2002). Another advantage is that the MWO maps are updated more than ten times per day, which significantly reduces the noise in the magnetic field measurements; in comparison, WSO and NSO (after the SOLIS magnetograph became operational in late 2003) update their maps up to three times per day (Arge *et al.*, 2004; Lee *et al.*, 2009a). Moreover, there are relatively fewer data gaps in the MWO data (Arge *et al.*, 2004; Lee *et al.*, 2009a).

The canonical value of 2.5 $R_\odot$ that is commonly used for the source surface in PFSS modeling is based on earlier works by Hoeksema, Wilcox, and Scherrer (1982, 1983) and Hoeksema and Scherrer (1986), although values between 1.5 $R_\odot$ and 3.5 $R_\odot$ have been discussed in studies by Levine *et al.* (1977), Schatten, Wilcox, and Ness (1969), and Altschuler and Newkirk (1969). It was the 2.5 $R_\odot$ value that gave the best overall agreement between the PFSS-inferred IMF polarities with those observed at Earth (Hoeksema, Wilcox, and Scherrer, 1983; Hoeksema, 1984). The smaller source surface values generally have been derived from soft X-ray images of coronal holes to better match the open flux geometry (see Levine *et al.*, 1977).

Our goal is to find a consistent picture based on the MWO observations together with PFSS modeling that describes both the solar sources and the interplanetary field for the cycle 23 minimum period, and to investigate what differences, if any, exist compared to the previous minimum. More specifically, we select the MWO data to develop a consistent picture of the sizes and shapes of the coronal holes seen in EUV images taken by the Extreme ultraviolet Imaging Telescope (EIT) on the *Solar and Heliospheric Observatory* (SOHO, Delaboudiniere *et al.*, 1995) and the Extreme Ultraviolet Imager (EUVI) of the *Solar TErrestrial RElations Observatory* (STEREO, Kaiser, 2005)/Sun Earth Connection Coronal and Heliospheric Investigation (SECCHI, Howard *et al.*, 2002) and the inferred IMF magnitude and polarity computed from the photospheric magnetic field that map to the source surface.

Our study proceeds as follows. In Section 3 we investigate the computed coronal hole footpoints for source surface values of 1.5, 1.8, and 2.5 $R_\odot$, which bracket the values generally used for PFSS modeling of the solar minimum period. We also show results of the PFSS calculations for the fraction of the open coronal areas and magnetic flux for the solar cycles 22 and 23 minimum periods, the values of which depend on the source surface height. In addition, we calculate the IMF values inferred from the PFSS results and compare them with those observed at Earth at 1 AU. For the *in situ* data, we use the OMNI data set available at http://omniweb.gsfc.nasa.gov/. Our comparison shows that the source surface height that produces the best values depends on the minimum period in question. We use the *in situ* measurements at 1 AU to infer the best overall source surface value that gives the observed IMF magnitudes and polarities. In Section 4, we also present a similar set of results using observations from the Michelson Doppler Imager (MDI) on board SOHO and compare the results with those based on MWO for the cycle 23 minimum period. In Section 5 we discuss our results and draw some conclusions about matters such as the relationship between the solar field and interplanetary field.

3. PFSS Model Results *versus* Observations

The bottom panels of Figures 4 and 5 show the comparison of extreme ultraviolet (EUV) synoptic maps from SOHO EIT and STEREO/SECCHI EUVI for Carrington rotations (CRs) 1914 and 2060, respectively. These rotations were chosen as representatives of the cycles 22 and 23 minimum periods. The top three panels progressing downward are the PFSS model open field footpoint regions for the three source surface radii of 1.5, 1.8, and

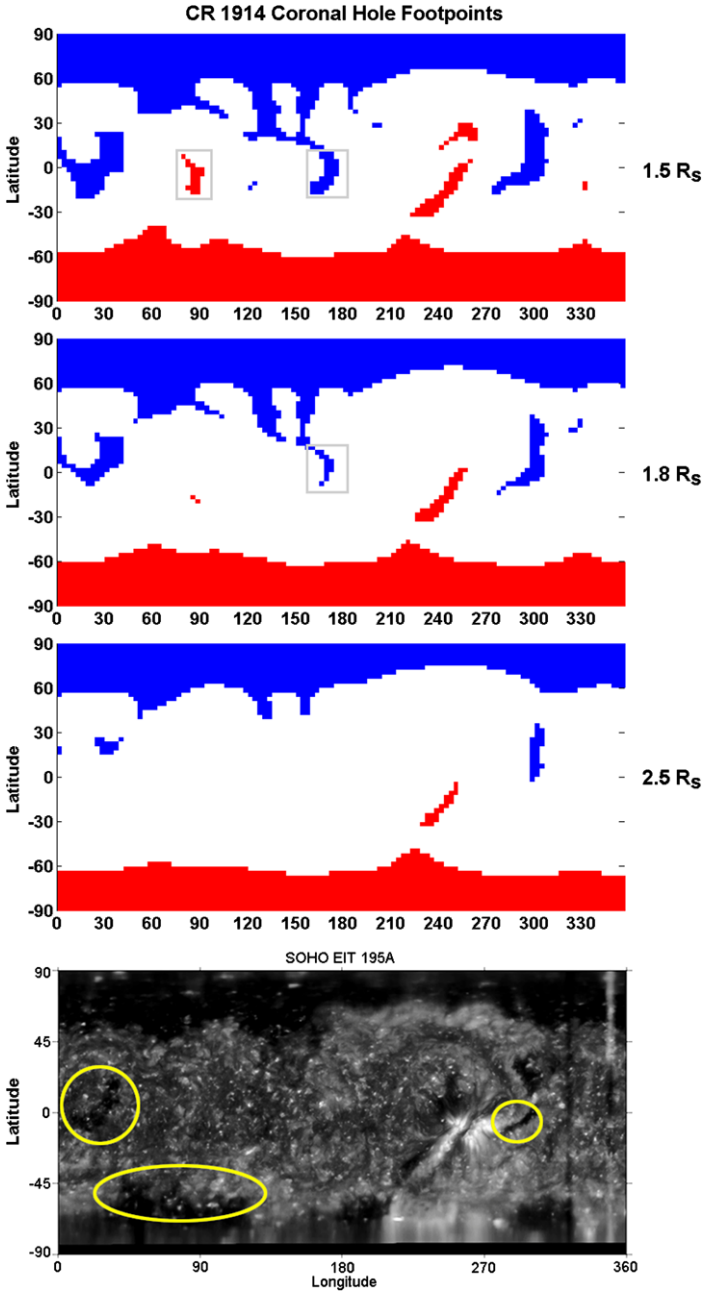

Figure 4 Comparison of PFSS results with 195 Å EUV map for CR 1914 (18 September to 15 October 1996) of cycle 22. For the PFSS modeling, we use solar observations from MWO and source surface heights of 1.5, 1.8, and 2.5 $R_{\odot}$. The yellow circles mark the gross coronal hole features that are largely missing from the 2.5 $R_{\odot}$ mapping results. The gray rectangles mark the gross features that appear in the mapping results but not in the EUV image. The red (blue) areas denote the negative inward (positive outward) field.

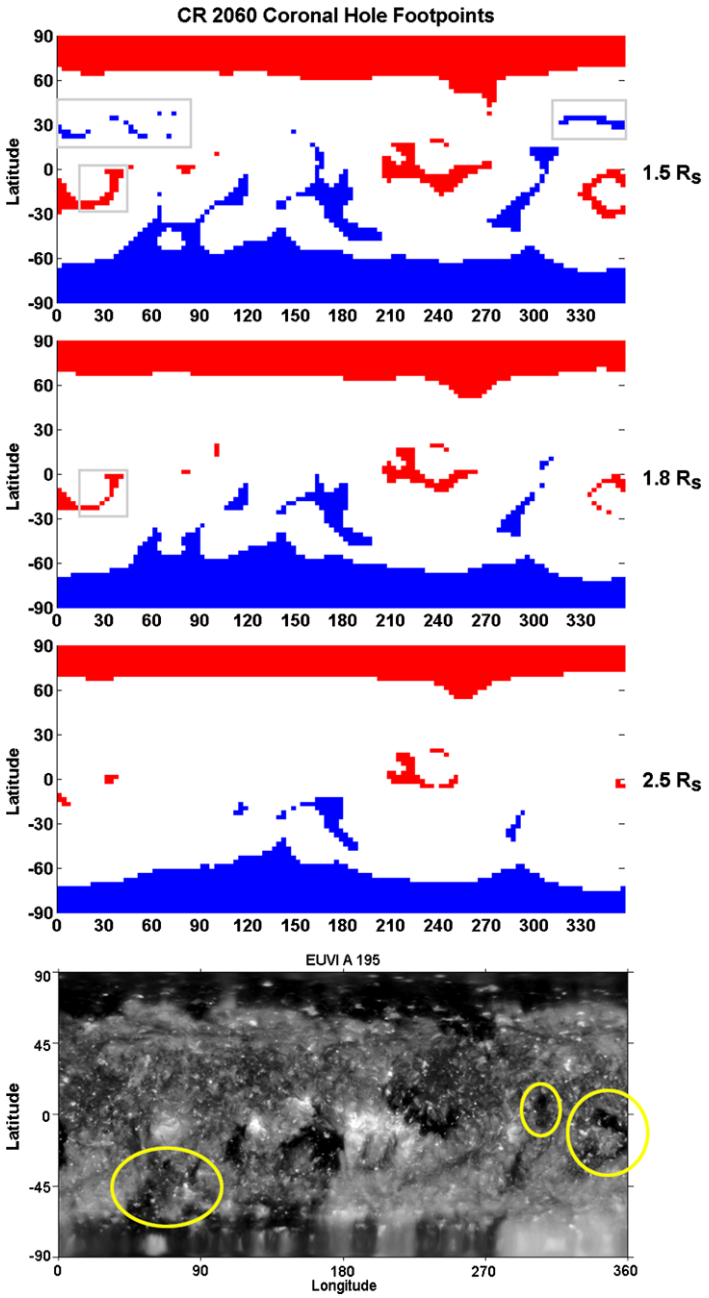

Figure 5 Same setup as in Figure 4, but for CR 2060 (14 August 2007 to 10 September 2007) of cycle 23.

2.5 $R_{\odot}$. The colors identify the radial field polarity in the open field or coronal hole areas (red for negative inward and blue for positive outward field lines) for the three selected source surface radii. A qualitative comparison between the observations in the EUV maps and the

different source surface maps suggests that the 2.5 $R_\odot$ source surface results are missing part of or entire coronal holes in both Carrington rotation examples, where the yellow circled areas in the EUV images show several clear omissions found in the 2.5 $R_\odot$ mapping (third panel from top in Figures 4 and 5). Although we do not show them here, this is also true for the other Carrington rotations within our minimum periods of study.

The mapping results suggest that a smaller source surface may be required to better approximate the observed open field regions. The comparison with the EUV maps shows that the 1.5 and 1.8 $R_\odot$ source surface results capture the coronal hole features that are omitted by the 2.5 $R_\odot$ results. However, note that the qualitative comparison shows that the smaller source surface results, especially those derived from using 1.5 $R_\odot$, produce coronal hole features (marked by gray rectangles) that are not observed. Out of these three source surface cases, the 1.8 $R_\odot$ source surface value appears to be a good compromise for capturing the coronal hole features that are observed. This radius is the better option for analyzing the possible implications for the interplanetary field and understanding how the photospheric field relates to it, at least at quiet times of the solar cycle. In reality, the source surface is most likely non-spherical, with a height that varies as a function of position (on the Sun) and in time. A model using a non-spherical source surface description has been developed for a dipolar (Schulz, Frazier, and Boucher, 1978) and a quadrupolar solar field configuration (Schulz, 2008). However, a few studies that utilized such a source surface description were restricted to modeling special cases since realistic multipolar magnetic field boundary conditions presented computational challenges (*e.g.*, Levine, Schulz, and Frazier, 1982; Schulz, 1997).

One additional point of note is the differences in the coronal holes for the cycles 22 and 23 minimum periods, which have been reported in recent studies. For the cycle 23 minimum period, the solar corona exhibited larger, long-lived, low-to-mid-latitude coronal holes (Lee *et al.*, 2009b; Luhmann *et al.*, 2009; Abramenko *et al.*, 2010), although the polar coronal hole areas were smaller in the north and the south (Kirk *et al.*, 2009). Moreover, Wang, Robbrecht, and Sheeley (2009) demonstrated that a larger fraction of flux is coming out of low-to-mid-latitude coronal holes for the cycle 23 minimum period than for cycle 22. Thus, photospheric fields that are not in the polar regions are especially important contributors to the interplanetary flux for the recent minimum.

In Figure 6a we show information about the total (unsigned) solar magnetic flux coming out of the photosphere as a function of time, as estimated from the twenty-order spherical harmonic coefficients derived from the MWO synoptic maps. The total photospheric flux for each Carrington rotation is calculated in the following manner: for each grid point in the PFSS model, we multiply the associated photospheric field value with the area element on the sphere (a function of the grid colatitude and grid size) and sum up the flux values. It can be seen that between the solar minimum and maximum periods, there is change by a factor of ten or more in the total photospheric flux. The figure highlights the small difference between the two cycle minimum periods shown in the gray-shaded regions (the selection based on comparable sunspot numbers), taking into account that the cycle 23 minimum period is longer. Within the shaded bands, the average photospheric field for cycle 23 is 0.35 μT compared with 0.384 μT for cycle 22. If the summed coronal hole areas in the Carrington maps are the same, we would expect the IMF to be different by their ratio of $\approx 8\%$. However, as shown in Figure 2 and also as reported in previous studies (*e.g.*, Lee *et al.*, 2009b), the difference in the average IMF values between the two minima is about 30%.

The fraction of the photosphere within coronal hole areas for each Carrington rotation is shown in Figure 6b. The values are computed from the three source surface radii (red for 1.5 $R_\odot$, blue for 1.8 $R_\odot$, and black for 2.5 $R_\odot$) for the entire period from the cycle 22

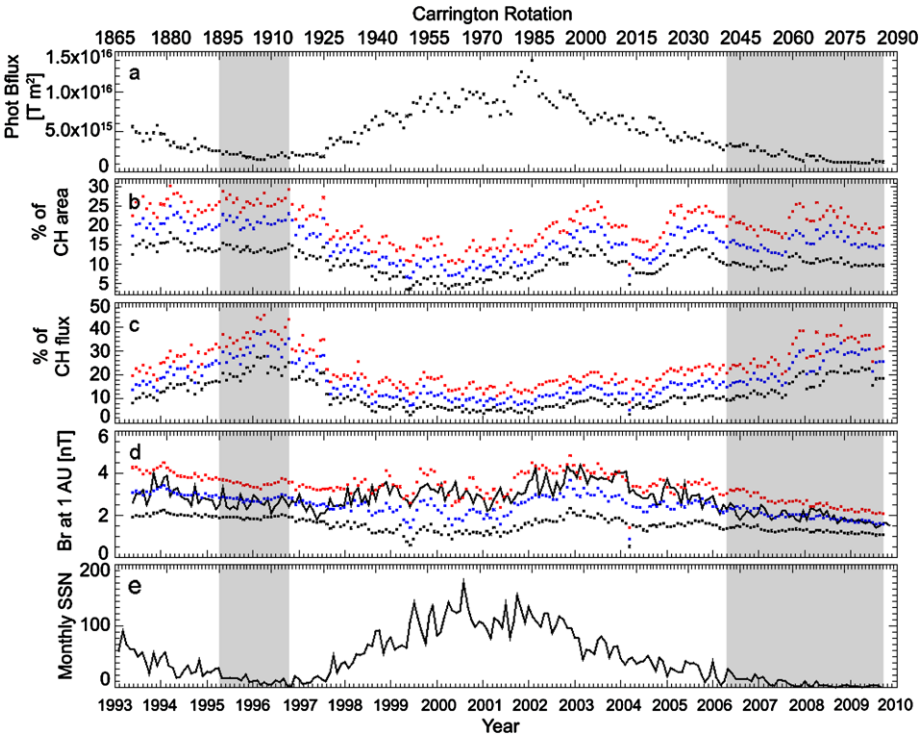

Figure 6 Based on MWO observations, we calculated the (a) total (unsigned) photospheric flux, (b) fraction of open coronal hole areas, (c) fraction of (unsigned) photospheric flux that maps into interplanetary space, (d) PFSS-inferred IMF at 1 AU *versus* Carrington rotation-averaged OMNI observations (solid black line), and (e) monthly sunspot numbers. The colors shown represent the different source surface heights utilized in the PFSS calculations: 1.5 (red), 1.8 (blue), and 2.5 (black) $R_{\odot}$. The gray-shaded regions mark the minimum periods (the selection based on comparable sunspot numbers), where the cycle 22 period is from CRs 1895 to 1915 (19 April 1995 to 10 November 1996) and the cycle 23 period is from CRs 2041 to 2086 (14 March 2006 to 4 April 2009).

declining phase to the cycle 23 minimum period (CRs 1864 to 2086). However, although we show them for completeness, we do not expect the solar maximum results (unshaded section in the center of the plot) with PFSS to be as accurate, and we do not discuss them here (see Riley *et al.* (2006) for such a discussion). As expected from PFSS modeling, the fractional areas of the coronal holes become larger as we decrease the source surface radius. During the solar minimum periods (gray-shaded regions), for a given source surface value the fraction of open area on the solar surface is smaller for the cycle 23 minimum compared to cycle 22. The difference is about 21%, 26%, and 27%, for source surface values of 1.5 $R_{\odot}$, 1.8 $R_{\odot}$, and 2.5 $R_{\odot}$, respectively, in spite of that fact that Abramenko *et al.* (2010) and Wang, Robbrecht, and Sheeley (2009) found the fractional coronal hole areas to be larger for the low-to-mid-latitude regions for the cycle 23 minimum period.

We show in Figure 6c the fraction of the (unsigned) photospheric flux that maps out to interplanetary space according to the PFSS model with the three source surface radii. The fractional value for each Carrington rotation is calculated by dividing the total flux at the source surface with the total flux emanating from the photosphere (Figure 6a). The total flux at the source surface is calculated in a similar manner to that described previously for the

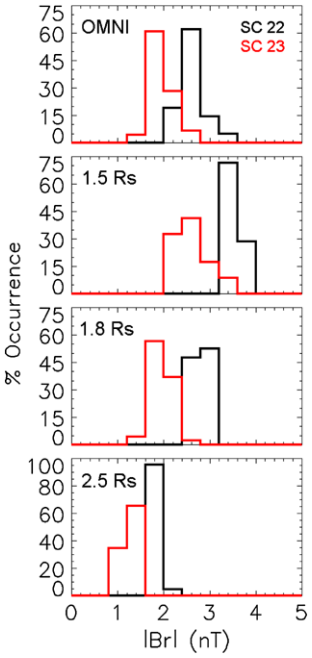

Figure 7 Histogram of occurrence for the Carrington rotation-averaged OMNI radial field at 1 AU and the PFSS-inferred results using the 1.5, 1.8, and 2.5 $R_\odot$ source surface values. The red and black data shown are for the solar cycles (SC) 23 and 22 minimum periods, respectively, where their time ranges are shown in Figure 6.

photospheric values, and is repeated for each source surface value used in this study (*e.g.*, 1.5 $R_\odot$, 1.8 $R_\odot$, and 2.5 $R_\odot$). We assume that all the heliospheric open flux originates in the coronal hole open field footpoints identified in the PFSS model. For a given source surface radius, the fraction mapped out has decreased for the cycle 23 minimum period in comparison to the previous one. Specifically, the flux decreased by about 19%, 23%, and 25% for source surface radii of 1.5 $R_\odot$, 1.8 $R_\odot$, and 2.5 $R_\odot$, respectively, during the cycle 23 minimum period. So although this minimum period has weaker globally integrated photospheric fields by about 8%, the general behavior of the open and closed photospheric fields and the fractional mapping of the photospheric fields into the heliosphere are quite different according to the PFSS modeling. We now ask whether the production of the measured interplanetary field strength, which is less for cycle 23 by about 30%, is determined in part by the height where the field lines become open as indicated by the source surface height itself.

In Figure 6d we compare the OMNI data with the PFSS-inferred radial IMF at 1 AU. The latter is calculated from the global source surface or open field flux under the assumption that radial IMF is independent of the heliographic latitude and varies in proportion to the (computed) open flux at the Sun (*e.g.*, see Smith and Balogh, 2008). The OMNI data (solid black line) for both minimum periods seems to be approximately described by the PFSS model when we use the source surface value of 1.8 $R_\odot$ (blue), although there is a slight suggestion of a larger source surface for the cycle 22 minimum period. We note that OMNI data have been averaged over one Carrington rotation in order to directly compare with the PFSS-inferred IMF values shown. Figure 7 further demonstrates that the 1.8 $R_\odot$ radius does the best of the three source surface radii in describing the IMF radial components at 1 AU in the solar minimum periods of this study. The histograms for the OMNI IMF (top panel) are similar to those shown earlier in Figure 2, but the data have been averaged over one Carrington rotation. Following the same color scheme, the red (black) histograms are generated from data for the cycle 23 (22) minimum period.

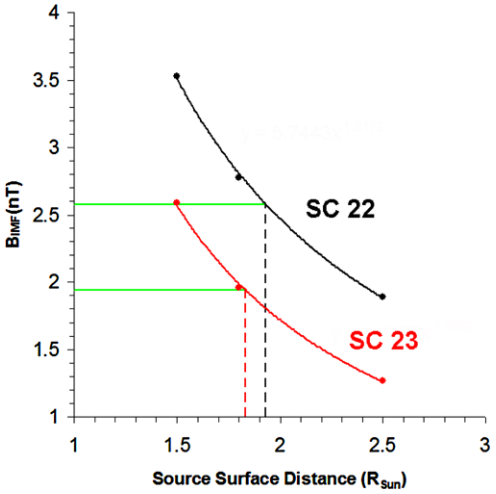

Figure 8 Best overall source surface values for solar cycle (SC) 23 (red) or 22 (black) inferred from the median OMNI IMF values (green) from each respective solar minimum period. We obtain 1.93 and 1.83 $R_\odot$ for cycles 22 and 23, respectively, from power law fits to the data as shown.

The small differences in the PFSS-inferred values for the two periods and the observations can be better understood from Figure 8. This figure shows the 1 AU IMF values predicted for each source surface radius for the data from each minimum period (dots connected by curves) compared to the average measured fields from the OMNI data (black for cycle 22, red for cycle 23). From power law fits to the data, the best source surface values for each minimum period are shown by the vertical dashed lines. The average *in situ* IMF values from cycles 22 and 23 (2.6 nT and 1.9 nT, respectively) are shown as green horizontal bars. From the black and red dashed vertical lines, we obtain the best source surface radii of 1.93 $R_\odot$ and 1.83 $R_\odot$ for cycles 22 and 23, respectively. From the difference in the source surface heights required to obtain the observed IMF values, it is evident that a small change in the source surface value could explain the significant difference in the observed IMF. This method provides a more accurate way of understanding the interplanetary field strength than simply looking at the ratio of the photospheric field without considering the coronal hole geometry and its outward mapping.

In addition to investigating the IMF strengths, we compare the PFSS-derived polarities with observations. Figures 9 and 10 show the polarity time series for a selection of Carrington rotations from cycles 22 and 23, respectively. In each figure, we use the daily averaged OMNI data which have been shifted backwards in time (a variable time shift based on the observed solar wind speed for each data element) such that the polarity values represent those at a distance of 2.5 $R_\odot$. In this comparison, to obtain a model resolution that is comparable to the daily averaged OMNI data, we generated PFSS results that have a grid spacing of $\approx 13.2°$ in the ϕ direction. For each set of Carrington groups shown in Figures 9 and 10, the OMNI data are shown in black in the top panel; in the bottom three panels we show the PFSS results for 2.5 $R_\odot$, 1.8 $R_\odot$, and 1.5 $R_\odot$ (black, blue, and red, respectively). If we compare the gross features of the observed and modeled polarities, the predicted values based on any of the three source surface values are quite comparable to the observations.

Using the same data set, in Figures 11 and 12 we examine more closely the number of sector boundary crossings that are observed and predicted. Here, we show the entire range of Carrington rotations that are within our minimum solar activity periods of study, where the OMNI data are shown as gray asterisks and the PFSS results for 2.5 $R_\odot$, 1.8 $R_\odot$, and 1.5 $R_\odot$ are shown, respectively, in black (closed circles), blue, and red (opened circles).

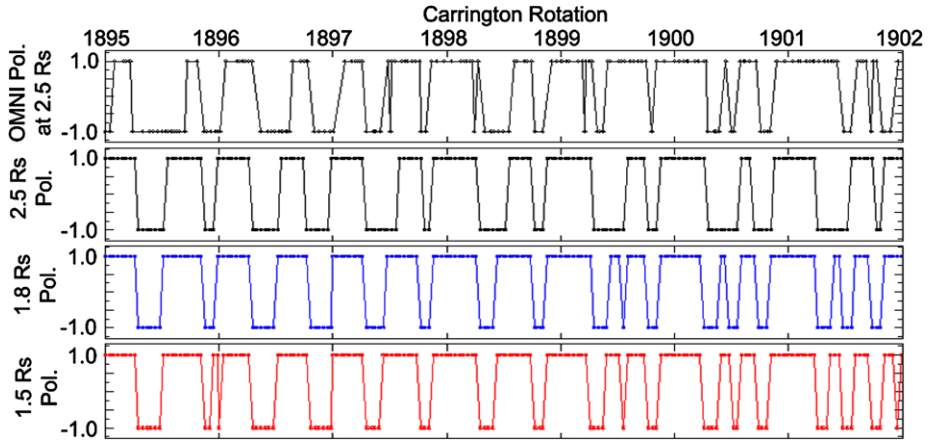

Figure 9 Daily averaged OMNI polarity data and PFSS results for a selection of Carrington rotations from the cycle 22 minimum period. Each set of time series shows (top) OMNI results projected back to 2.5 $R_\odot$ (black), together with the PFSS-derived polarities from source surface radius of (second) 2.5 $R_\odot$ in black, (third) 1.8 $R_\odot$ in blue, and (bottom) 1.5 $R_\odot$ in red.

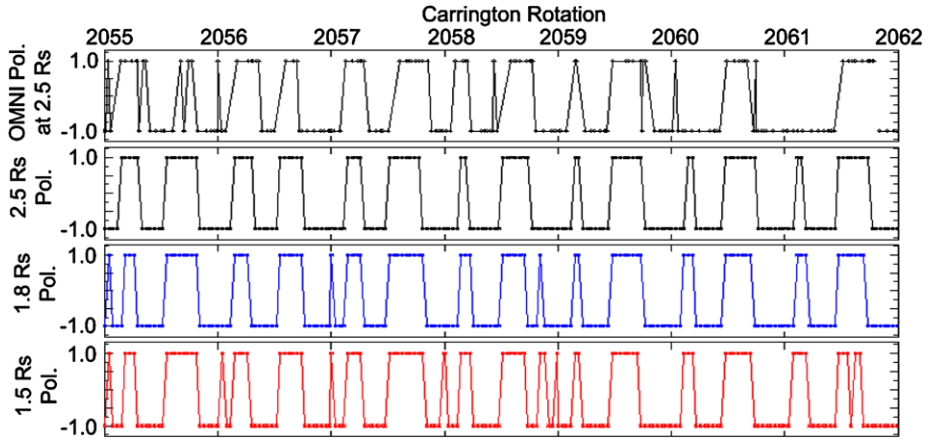

Figure 10 Daily averaged OMNI polarity data and PFSS results for a selection of Carrington rotations from the cycle 23 minimum period. Each set of time series shows (top) OMNI results projected back to 2.5 $R_\odot$ (black), together with the PFSS-derived polarities from source surface radius of (second) 2.5 $R_\odot$ in black, (third) 1.8 $R_\odot$ in blue, and (bottom) 1.5 $R_\odot$ in red.

When we compare the PFSS results based on 2.5 $R_\odot$ for both solar minimum periods, the matches of the sector boundary crossings with the observations are very poor at best, with some improvements to the matches if a smaller source surface is used instead. More specifically, when using 2.5 $R_\odot$, the number of mismatches that occur is about 70% (76%) for the cycle 22 (23) minimum period. Of these, about 20% (12%) of the sector crossings are matched by using one or both of the smaller source surface values. In the case when there is a match between the observations and the 2.5 $R_\odot$ results, there is also a match with the results based on one or both of the smaller values. This occurred about 25% (17%) of the

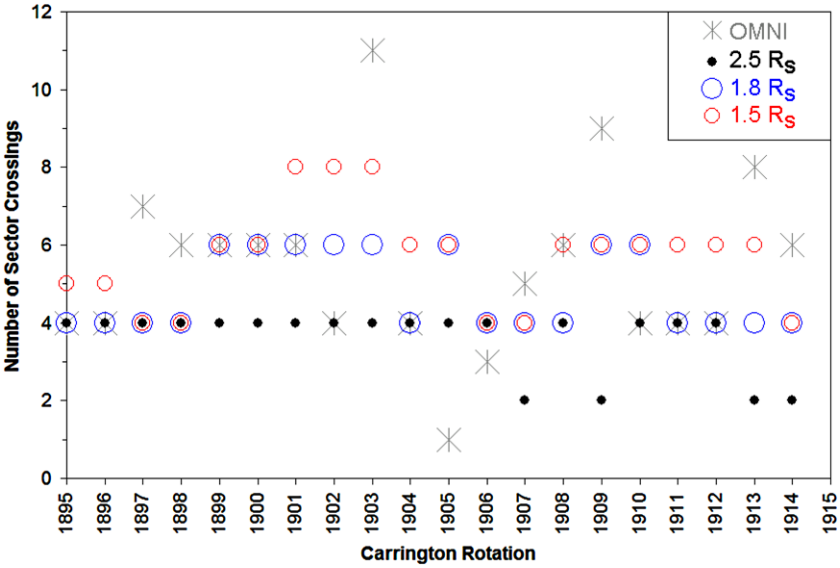

Figure 11 Statistics for CRs 1895 to 1915 of the cycle 22 minimum period, showing the number of sector boundary crossings for the daily averaged OMNI data (gray asterisk) and the PFSS-derived polarities (2.5 $R_\odot$ in black, 1.8 $R_\odot$ in blue, and 1.5 $R_\odot$ in red).

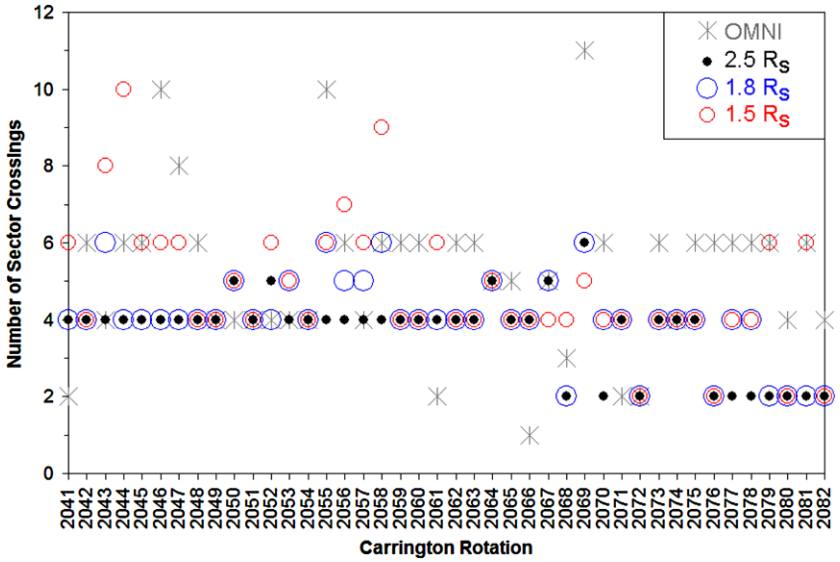

Figure 12 Statistics for CRs 2041 to 2082 of the cycle 23 minimum period, showing the number of sector boundary crossings for the daily averaged OMNI data (gray asterisk) and the PFSS-derived polarities (2.5 $R_\odot$ in black, 1.8 $R_\odot$ in blue, and 1.5 $R_\odot$ in red).

time for the cycle 22 (23) minimum study period. Based on these statistics, the canonical 2.5 $R_\odot$ source surface value does not appear to agree with the sector crossing observations as often as a smaller source surface value for the periods studied.

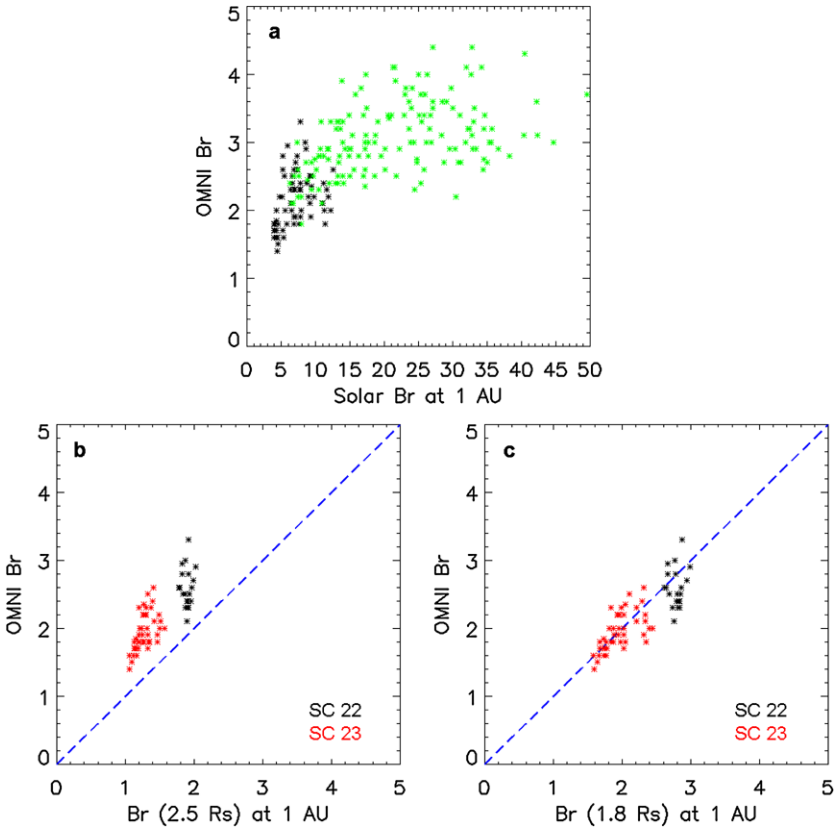

Figure 13 Correlation of the IMF values from *in situ* 1-AU observations and PFSS-derived results. (a) Comparison of the *in situ* IMF with the photospheric field values projected out to 1 AU, for CRs 1865 to 2086. The black color marks the solar minimum period data shown in the gray-shaded regions in Figure 6, whereas the green color marks data outside this period. (b) *In situ* IMF with the PFSS-inferred IMF using the 2.5 $R_{\odot}$ source surface radius. Here we only show the data for the solar cycles (SC) 22 and 23 minimum periods, color coded in red and black, respectively. (c) The same type of plot for the 1.8 $R_{\odot}$ source surface radius. Values shown are in nanoteslas.

Overall, the analyses of the IMF magnitudes and polarities described above suggest that a smaller source surface radius than 2.5 $R_{\odot}$ should be used in the PFSS model applications during periods of low solar activity. This is consistent with the earlier findings by Schatten, Wilcox, and Ness (1969), Levine (1982), and Levine *et al.* (1977), where the smaller source surface heights in the PFSS modeling produced results that better matched with observations of the open magnetic field during the cycle 20 minimum period. For our study, where we used solar observations from MWO, the 1.8 – 1.9 $R_{\odot}$ source surface radius seems the most appropriate value to use in PFSS model applications in the cycles 22 and 23 minimum periods, for this comparison. To further illustrate this, we correlate our PFSS results with the individual Carrington rotation-averaged IMF observations, shown in Figure 13. In panel a, we compare the interplanetary field observed at 1 AU with those derived from the total solar photospheric flux for the entire period shown in Figure 6 (CRs 1865 to 2086). For the IMF values calculated from the total photospheric flux, we utilize flux conservation and determine the IMF values for a sphere with a radius of 1 AU. The green dots indicate the

data shown in the unshaded portion of Figure 6, which is largely the solar maximum period, while the black dots mark the data from the minimum periods. The factor of ten spread in the photospheric values that are projected out to 1 AU (*e.g.*, the values shown in the x-direction) is consistent with the spread in the photospheric flux values derived for the solar minimum and maximum periods shown in Figure 6a. Figures 13b and 13c illustrate the departure from proportionality if we simply assume a direct relationship between the observed solar magnetic field and the measured IMF, not taking into account the areas (size and shape) and the locations of the coronal holes. In Figure 13b we plot values for only the minimum periods (red for cycle 23, black for cycle 22) as shown by the shaded regions in Figure 6 using the OMNI data set and the PFSS-derived results based on the commonly used source surface radius of 2.5 $R_{\odot}$. Overall, the correlation with the observed IMF is not centered on the slope 1 line (blue dashed line). However, the correlation with the PFSS-derived values based on the source surface radius of 1.8 $R_{\odot}$, shown in Figure 13c, is much closer to 1:1. Here, the spread in the IMF values in the y-direction for the cycle 22 minimum period is modestly larger ($\approx$11%) in comparison to the spread in the values for the cycle 23 period ($\approx$ 8%).

4. Comparison with MDI Measurements for Cycle 23

Our selection of MWO data used for this study was based on its established consistency over solar cycles, higher spatial resolution, and larger number of updates to magnetograms, compared to other solar observatories (*e.g.*, NSO, WSO). Assuming all factors to be equal, we expect the general conclusions pertaining to the source surface height to be similar if we use data from other solar observatories (*cf.* Arge *et al.*, 2002). In this section, we compare the MWO-derived PFSS results for the cycle 23 minimum period with similar results obtained using observations from the Michelson Doppler Imager (MDI) instrument (Scherrer *et al.*, 1995) on board the SOHO spacecraft. We chose to use the MDI observations for this comparison because the data have been intercalibrated with observations from MWO and are publicly available on the MDI webpage. In particular, the MDI observations have been adjusted for spatial, spectral, and temporal issues based on the techniques developed by Tran *et al.* (2005) and Liu, Zhao, and Hoeksema (2004).

Figure 14 shows a qualitative comparison of the open coronal hole regions for CR 2060 imaged by STEREO/EUVI with the PFSS mapping results based on MDI observations. As before, the yellow-circled areas in the EUV images show omissions of gross features when using the source surface value of 2.5 $R_{\odot}$, whereas the gray rectangles mark the features mapped by PFSS that are not observed. The MDI-based results shown are similar to the results based on the MWO observations shown in Figure 5. Specifically, the MDI results also suggest a smaller source surface value for approximating the observed open field regions. However, we note that the MDI mapping results appear to better capture some of the details of the gross coronal holes features when we use the source surface value of 1.5 $R_{\odot}$, rather than the 1.8 $R_{\odot}$ value found for MWO.

In Figures 15a and 15c, we show the calculated total (unsigned) open photospheric flux for each Carrington rotation in the cycle 23 minimum period, based on the source surface values of 1.5 $R_{\odot}$ and 1.8 $R_{\odot}$, respectively. The blue (red) symbols show the results based on the MDI (MWO) observations. For both source surface cases (panels a and c), the amount of open flux calculated by PFSS is different, depending on which sets of solar observations are used. In particular, the MWO open flux values are on average about 50% greater than the MDI values.

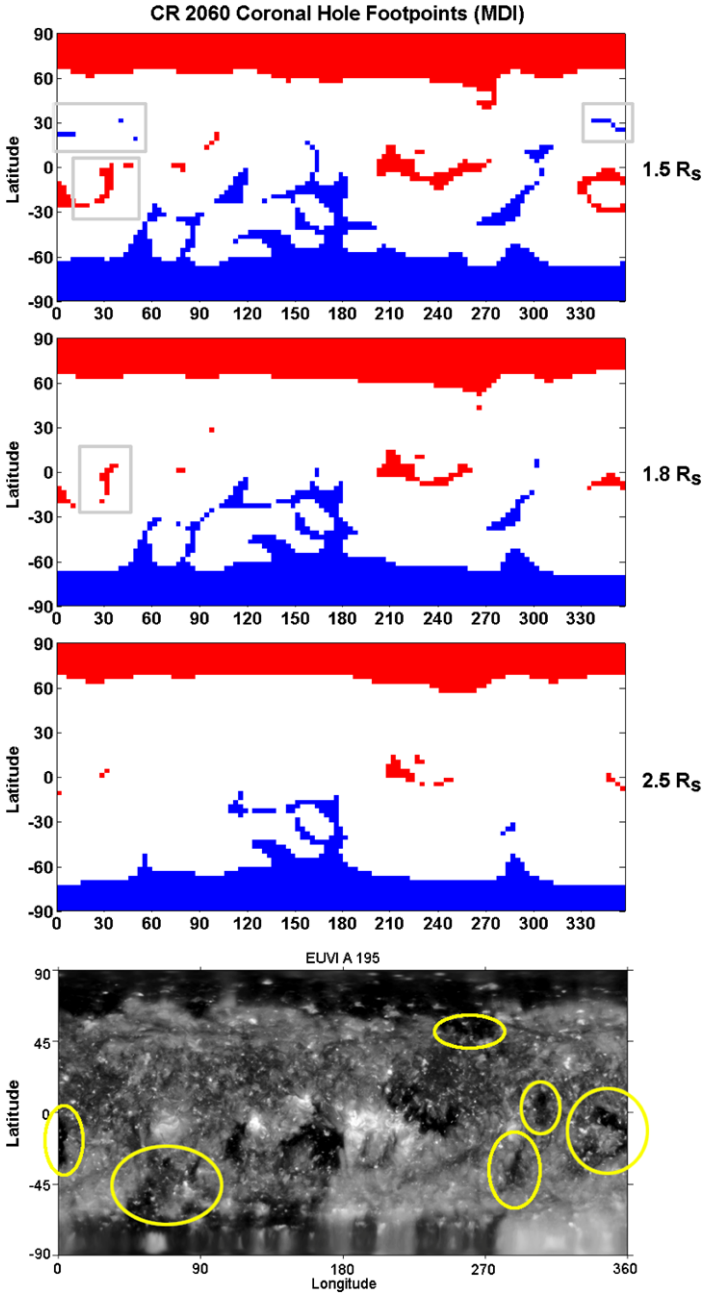

Figure 14 Same as for Figure 5 for CR 2060 (14 August 2007 to 10 September 2007) of cycle 23, but here we use solar observations from MDI. The yellow circles mark the gross coronal hole features that are largely missing from the 2.5 $R_{\odot}$ mapping results. The gray rectangles mark the gross features that appear in the mapping results but not in the EUV image. The red (blue) areas denote the negative inward (positive outward) field.

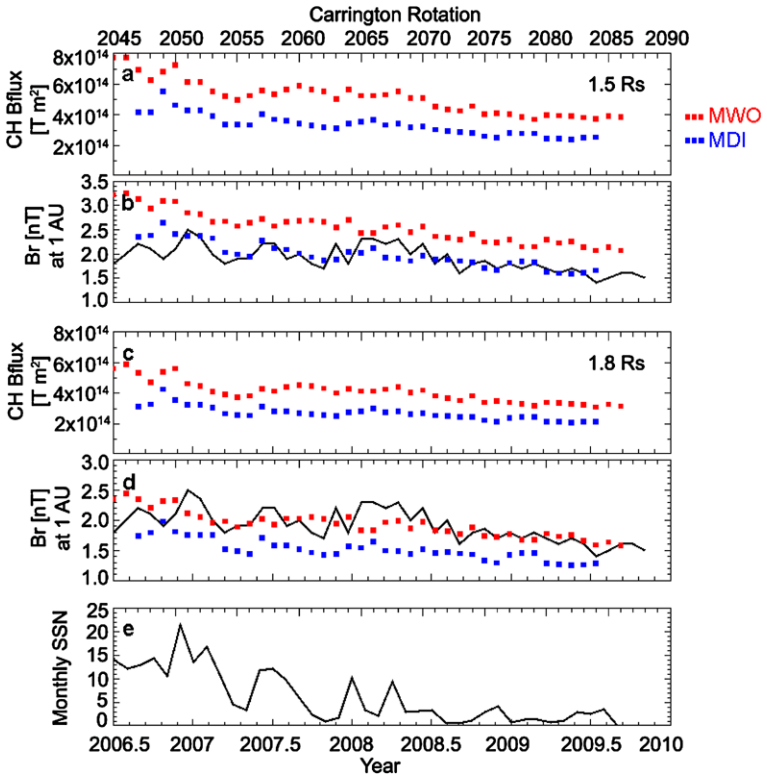

Figure 15 Calculations based on MWO (red) and MDI (blue) observations. Using the source surface value of 1.5 $R_{\odot}$, we show in panels (a) and (b) the calculations for the total (unsigned) photospheric flux emanating from the coronal holes and the PFSS-inferred IMF at 1 AU *versus* Carrington rotation-averaged OMNI observations (solid black line), respectively. Similar calculations are shown in panels (c) and (d) using the source surface value of 1.8 $R_{\odot}$. The monthly sunspot numbers are shown in panel (e).

Panels b and d of Figure 15 show the 1.5 $R_{\odot}$ and 1.8 $R_{\odot}$ PFSS-inferred radial IMF values at 1 AU, respectively. For both source surface cases, the MWO radial magnetic field values are greater than the MDI values by about 30%. Thus, when we compare the inferred radial field values with the *in situ* 1 AU OMNI data (solid black line in panels b and d), the MDI results compare best with the OMNI data if the source surface value of 1.5 $R_{\odot}$ is used (panel b, blue symbols) rather than the source surface value of 1.8 $R_{\odot}$ (panel d, blue symbols). This is consistent with the suggestion for the smaller 1.5 $R_{\odot}$ source surface value when we compare the observed open field regions with the PFSS-mapped results as shown in Figure 14 for CR 2060. The suggestion for a source surface value of 1.5 $R_{\odot}$ when using MDI observations in PFSS modeling applications is further illustrated in Figure 16a, where we correlate the PFSS results for the cycle 23 minimum period with the individual Carrington rotation-averaged IMF observations. The correlation is closer to 1:1 when using MDI observations (blue) in comparison to MWO observations (red). As before (*e.g.*, see Figure 13), we illustrate the departure from proportionality if we assume a direct relationship between the observed photospheric magnetic field and the measured IMF at 1 AU and do not take into account the sizes, shapes, and locations of the coronal hole regions. Figure 16b

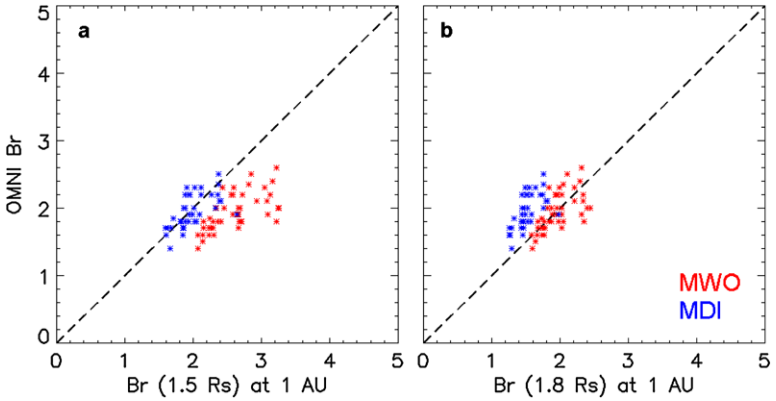

Figure 16 Correlation of the IMF values from *in situ* 1-AU observations and PFSS-derived results using solar observations from MDI (blue) and MWO (red). Panels (a) and (b) show the *in situ* IMF with the PFSS-inferred IMF using source surface values of 1.5 $R_\odot$ and 1.8 $R_\odot$, respectively. Values shown are in nanoteslas.

shows the correlation of the observed and inferred IMF values when using the source surface value of 1.8 $R_\odot$.

Overall, our MWO- and MDI-based PFSS results suggest a smaller source surface value that is contrary to the surface value of 2.5 $R_\odot$. However, the source surface value of $\approx$1.5 $R_\odot$ is suggested by the MDI results, whereas the value of $\approx$ 1.8 $R_\odot$ is suggested by the MWO results. The difference in our results is due to the use of solar observations from different observatories. Although the MDI data have been intercalibrated with MWO observations, the comparison is still not 1:1 for the reasons stated in Section 2. In general, the influence of the data from different solar observatories on our final conclusions is an important issue. However, the necessary corrections and modifications that should be applied to the observations for such a comparison prior to analysis is intrinsically complicated (*cf.* Arge *et al.*, 2002) and is beyond the scope of this paper. The results presented in this study are nonetheless robust in that they produce a consistent picture of both coronal holes and the IMF when a smaller source surface radius is used in the PFSS model.

5. Conclusions

In this study, our goal was to build a consistent picture based on the MWO observations together with PFSS modeling that described both the solar sources and the interplanetary field for the cycle 23 minimum period, and to investigate the differences (and similarities) compared to the previous cycle 22 minimum. We took the approach of invoking a source surface height in the PFSS model that is smaller than the canonical value of 2.5 $R_\odot$, motivated by frequent improved agreement between the EUV images and the modeled open field regions. This approach was also used in the earlier studies by Schatten, Wilcox, and Ness (1969), Levine (1982), and Levine *et al.* (1977), where smaller source surface heights in their PFSS modeling produced results that better matched with soft X-ray coronal hole images during the cycle 20 minimum period. When using solar observations from MWO, we find that the use of a smaller source surface radius of $\approx$ 1.8 $R_\odot$ makes a significant difference in the estimation of the IMF strength from the PFSS model for the cycle 23 minimum

period, with a slightly larger value of $\approx 1.9\ R_{\odot}$ for the cycle 22 minimum period, as suggested in Figure 8. Moreover, the use of these small radii often more closely approximates the observed numbers of the polarity sector crossings. In using a different set of solar observations from MDI as a comparison, we find that the source surface radius of $1.5\ R_{\odot}$ did a better job in the estimation of the IMF strength for the cycle 23 minimum period from the PFSS model, rather than the value of $1.8\ R_{\odot}$ suggested when we use observations from MWO. Despite this difference, our conclusion that a smaller source surface value should be used in modeling applications for the cycle 23 minimum period remains the same.

A smaller source surface height for the cycle 23 minimum period compared to the previous one is consistent with the MHD equations for the location of the cusp point of the coronal streamer, as discussed in the study by Pneumann and Kopp (1971). If the cusp location is used as a proxy for the source surface height, Equation (1) from that study suggests that the weaker solar fields will produce cusp points that are closer to the solar surface; *e.g.*, the source surface height will be lower. Since the cusp height indicates where the field lines become open, the height at which the energy balance between the magnetic field and plasma changes will also be lower. In general, our results (see also Steinolfson, Suess, and Wu, 1982) suggest that the coronal pressure is not strongly dependent on the photospheric field in the largest-scale loops and open field regions, but that instead, the photospheric field strength and distribution control the solar wind fluxes by determining the source regions (location and area).

Several conclusions from this study are of potential practical use.

i) Several factors must be considered when inferring the interplanetary field strength from photospheric field strength, including the locations of the open fields (polar latitudes *versus* low-to-mid latitudes) and the sizes of the open field areas. Thus, in any PFSS modeling application that presumes one source surface height without some careful consideration of the mapping details, the results should be viewed with some caution.

ii) As Figure 8 illustrates, a small change in source surface height reduces the differences between modeled and observed IMF values. This suggests that the source surface height is changing over time and that the energy balance may be different from one minimum to the next, depending on both the polar and overall photospheric field strengths as well as the open field topology. Thus, simply taking changes of the photospheric fields as a measure of the change in the IMF (as in panel a of Figure 13) is inadvisable. From a modeling perspective, it would be useful to find a way of constraining an optimum source surface radius from observations without having to make a comparison after the fact. In the meantime, future PFSS modeling efforts (*e.g.*, that of Wang, Robbrecht, and Sheeley, 2009) should probably treat the source surface height as another parameter, especially when trying to predict long-term trends.

iii) In a previous study, Lee *et al.* (2009a) found that the numerical model-generated values for the magnetic components of the total field were often underestimated by a factor of two. It is possible that the boundary conditions, such as the source surface height of $2.5\ R_{\odot}$, used to drive the coronal component of the coupled corona-solar wind models could contribute to the underestimation of the magnetic field values. This will need to be tested in the near future by the model developers, possibly by using the smaller source surface values derived from this study in future model calculations and comparing the values with observations.

Acknowledgements The authors thank the NASA Goddard Space Flight Center Space Physics Data Facility (SPDF) and the National Space Science Data Center (NSSDC) for providing the OMNI data and OMNIWeb access, the Mount Wilson Observatory for providing access to their magnetogram data sets, and the agencies sponsoring these archives (NASA, NSF, USAF). The authors would like to acknowledge that SOHO

is a project of international cooperation between the European Space Agency and NASA. In addition, the authors wish to express thanks to Luca Bertello, Yang Liu, and Jack W. Harvey for their informal discussions with us regarding observations from different solar observatories, and for their encouragement to write this paper using data from MWO.

Christina O. Lee thanks the editor and the referee for their assistance in evaluating this paper.

This research was supported by the CISM project, which is funded by the STC Program of the National Science Foundation under agreement number ATM-0120950.

References

Abramenko, V., Yurchyshyn, V., Linker, J., Mikic, Z., Luhmann, J.G., Lee, C.O.: 2010, *Astrophys. J.* **712**, 813.

Altschuler, M.D., Newkirk, G.: 1969, *Solar Phys.* **9**, 131.

Arge, C.N., Pizzo, V.J.: 2000, *J. Geophys. Res.* **105**, 10465.

Arge, C.N., Hildner, E., Pizzo, V.J., Harvey, J.W.: 2002, *J. Geophys. Res.* **107**(A10), SSH16-1.

Arge, C.N., Luhmann, J.G., Odstrcil, D., Schrijver, C.J., Li, Y.: 2004, *J. Atmos. Solar-Terr. Phys.* **66**, 1295.

Balogh, A., Beek, T.J., Forsyth, R.J., Hedgecock, P.C., Marquedant, R.J., Smith, E.J., Southwood, D.J., Tsurutani, B.T.: 1992, *Astron. Astrophys. Suppl.* **92**, 221.

Balogh, A., Smith, E.J., Tsurutani, B.T., Southwood, D.J., Beek Forsyth, R.J., Horbury, T.S.: 1995, *Science* **268**, 1007.

Bame, S.J., McComas, D.J., Barraclough, B.L., Phillips, J.L., Sofaly, K.J., Chavez, J.C., Goldstein, B.E., Sakurai, R.K.: 1992, *Astron. Astrophys. Suppl.* **92**, 237.

Delaboudiniere, J.P., Artzner, G.E., Brunaud, J., Gabriel, A.H., Hochedez, J.F., Millier, *et al.*: 1995, *Solar Phys.* **162**, 291.

Hoeksema, J.T.: 1984, Structure and Evolution of the Large Scale Solar and Heliospheric Magnetic Fields, Ph.D. Thesis, Stanford University.

Hoeksema, J.T.: 2010, In: Kosovichev, A.G., Andrei, A.H., Rozelot, J.-P. (eds.) *Solar and Stellar Variability: Impact on Earth and Planets*, *IAU Symp.* **264**, 222.

Hoeksema, J.T., Scherrer, P.H.: 1986, *Solar Phys.* **105**, 205.

Hoeksema, J.T., Wilcox, J.M., Scherrer, P.H.: 1982, *J. Geophys. Res.* **87**, 10331.

Hoeksema, J.T., Wilcox, J.M., Scherrer, P.H.: 1983, *J. Geophys. Res.* **88**, 9910.

Howard, R.A., Moses, J.D., Socker, D.G., Dere, K.P., Cook, J.W.: 2002, *Adv. Space Res.* **29**, 2017.

Kaiser, M.: 2005, *Adv. Space Res.* **36**, 1483.

Kirk, M.S., Pesnell, W.D., Young, C.A., Hess Weber, S.A.: 2009, *Solar Phys.* **257**, 99.

Lee, C.O., Luhmann, J.G., Odstrcil, D., MacNeice, P.J., de Pater, I., Riley, P., Arge, C.N.: 2009a, *Solar Phys.* **254**, 155.

Lee, C.O., Luhmann, J.G., Zhao, X.P., Liu, Y., Riley, P., Arge, C.N., Russell, C.T., de Pater, I.: 2009b, *Solar Phys.* **256**, 345.

Levine, R.H.: 1982, *Solar Phys.* **79**, 203.

Levine, R.H., Altschuler, M.D., Harvey, J.W., Jackson, B.V.: 1977, *Astrophys. J.* **215**, 636.

Levine, R.H., Schulz, M., Frazier, E.N.: 1982, *Solar Phys.* **77**, 363.

Liu, Y., Zhao, X., Hoeksema, T.: 2004, *Solar Phys.* **219**, 39.

Luhmann, J.G., Li, Y., Arge, C.N., Gazis, P.R., Ulrich, R.: 2002, *J. Geophys. Res.* **107**(A8), SMP 3-1.

Luhmann, J.G., Lee, C.O., Li, Y., Arge, C.N., Galvin, A.B., Simunac, K., Russell, C.T., Howard, R.A., Petrie, G.: 2009, *Solar Phys.* **256**, 285.

McComas, D.J., Ebert, R.W., Elliott, H.A., Goldstein, B.E., Gosling, J.T., Schwadron, N.A., Skoug, R.M.: 2008, *Geophys. Res. Lett.* **35**, L18103.

Pneumann, G.W., Kopp, R.A.: 1971, *Solar Phys.* **18**, 258.

Riley, P., Linker, J.A., Mikic, Z., Lionello, R., Ledvina, S.A., Luhmann, J.G.: 2006, *Astrophys. J.* **653**, 1510.

Schatten, K.H.: 1971, *Cosm. Electrodyn.* **2**, 232.

Schatten, K.H., Wilcox, J.M., Ness, N.F.: 1969, *Solar Phys.* **6**, 442.

Scherrer, P.H., Bogart, R.S., Bush, R.I., Hoeksema, J.T., Kosovichev, A.G., Schou, J., *et al.*: 1995, *Solar Phys.* **162**, 129.

Schulz, M.: 1997, *Ann. Geophys.* **15**, 1379.

Schulz, M.: 2008, AGU Spring Meeting, SH44A-04.

Schulz, M., Frazier, E.N., Boucher, D.J. Jr.: 1978, *Solar Phys.* **60**, 83.
Smith, E.J., Balogh, A.: 2008, *Geophys. Res. Lett.* **35**, L22103.
Steinolfson, R.S., Suess, S.T., Wu, S.T.: 1982, *Astrophys. J.* **255**, 730.
Tran, T., Bertello, L., Ulrich, R.K., Evans, S.: 2005, *Astrophys. J. Suppl.* **156**, 295.
Ulrich, R.K., Evans, S., Boyden, J.E., Webster, L.: 2002, *Astrophys. J.* **139**, 259.
Wang, Y.M., Sheeley, N.R.: 1992, *Astrophys. J.* **392**, 310.
Wang, Y.M., Robbrecht, E., Sheeley, N.R.: 2009, *Astrophys. J.* **707**, 1372.
Zhao, X.P., Hoeksema, J.T.: 1995, *J. Geophys. Res.* **100**, 19.